

Research Article

4D Printed Shape Memory Polymers: Morphology and Fabrication of a Functional Antenna

Trenton Cersoli¹, Muneer Barnawi¹, Kerry Johnson¹, Edward Burden¹, Frank Li¹, Eric MacDonald², Pedro Cortes^{1,*}

1. Engineering Department, Youngstown State University, OH, 44555, USA; E-Mails: tmcersoli@student.ysu.edu; mibarnawi@student.ysu.edu; kjohnson10@student.ysu.edu; erburden@ysu.edu; xli@ysu.edu; pcortes@ysu.edu
2. Mechanical Engineering, The University of Texas at El Paso, TX, 79968, USA; E-Mail: emac@utep.edu

* **Correspondence:** Pedro Cortes; E-Mail: pcortes@ysu.edu

Academic Editor: Yifei Jin

Special Issue: [3D Printing of Engineering Materials](#)

Recent Progress in Materials
2022, volume 4, issue 2
doi:10.21926/rpm.2202009

Received: February 17, 2022
Accepted: April 25, 2022
Published: April 29, 2022

Abstract

Shape memory polymers (SMPs) are smart materials that can respond to certain thermal, chemical or electrical stimuli by inducing a structural conformation change into a temporary shape. In this work, a 3D printing process based on a Vat Photo-polymerization of a shape memory polymer (SMP) was investigated to produce customized smart and complex morphable antennas. The mechanical and material properties were examined through a tensile, flexural and rheological testing for different polymer mixture ratios. It was observed that the combination of 20% of an elastomeric resin in a thermoset UV system yields the highest shape recovery performance. The fabrication process of the antenna was based on the incorporation of a conductive material. The approach involved the inclusion of a thin copper electroplating technique. The radiofrequency performance of the fabricated antenna was examined by a vector network analyzer (VNA) and it was observed that a thermal stimulus



© 2022 by the author. This is an open access article distributed under the conditions of the [Creative Commons by Attribution License](#), which permits unrestricted use, distribution, and reproduction in any medium or format, provided the original work is correctly cited.

was capable of inducing a conformal shape on the antenna, resulting in a multi-radio frequency morphing system. The antenna performance was simulated in Ansys HFSS.

Keywords

4D printed shape memory polymer; vat photo-polymerization; modeling; morphing structures; electroplating

1. Introduction

With the growth of new materials and new manufacturing techniques, additive manufacturing (also known as 3D printing), shows the potential as a useful manufacturing technique for both new and traditional materials. Additive manufacturing offers several advantages over traditional manufacturing, specifically in producing parts at a reduced cost, with complex geometries, and a diversity of materials [1-3]. Additive manufacturing techniques fall into seven main categories that can be used to process different materials from ceramics, to metals, polymers, and composites [4-6]. One specific additive manufacturing technique for polymers is vat photopolymerization (VPP), which includes stereolithography (SLA), and digital light processing (DLP) technologies. In the case of VPP, a stage (on the z-axis) moves into a vat of liquid photopolymer resin, where a light source photo-crosslinks the resin to harden it. The motorized stage then moves up (or down) for the next layer of the object to be irradiated until the entire part is built in a layer-by-layer fashion. The main difference between DLP and SLA techniques is that SLA printers utilize a laser as the light source compared to a light-emitting diode (LED) or digital projection as the light source in DLP printers [7].

Of the wide range of materials available for additive manufacturing, smart materials (specifically shape memory polymers), are of specific interest. Unlike common materials, smart materials exhibit non-static material properties that can be used for sensing and actuation functions [8]. Smart materials can be responsive to various stimuli including: thermal, magnetic, electrical, and light stimuli [9]. Shape memory polymers are a class of these smart materials, and possess the ability to recover a permanent shape from a temporary fixed shape. In cases where weight and compactness are of the utmost importance, shape memory polymers can offer weight and space savings compared to traditional materials. In the aerospace industry, shape memory polymers are investigated for the fabrication of large deployable booms, and antennas for in-flight vehicles [10, 11].

Possessing the ability to shift between a temporary and a permanent shape, shape memory polymers can be used in the fabrication of antennas, where deployable and reconfigurable structures can save space, and elicit different radio frequency behavior. Jape et al created an origami based antenna that utilized shape memory polymer hinges to create a “self-foldable” reflector antenna [12]. The use of shape memory polymers as composite hinges for deployable truss structures has also been investigated, and often utilizes the rigidity of other materials to make a functional part [13, 14]. Furthermore, Ze et al. fabricated a helical antenna of magnetic-responsive shape memory polymers that could morph into different patterns that tune the antenna resonance frequency from 2.15 to 3.26 GHz [15].

Thermally-stimulated shape memory polymers are able to recover the permanent shape, often set during the manufacturing of the part. To apply a secondary shape, the part is heated above its transition temperature, often associated with the glass transition temperature (T_g) of the material, followed by an external load to induce deformation. Once the deformation is applied, the part can be cooled below its transition temperature under the constant load. Once the system is cooled the load can be removed, and the deformed part is in a stable secondary shape. In the absence of an external load, the part will revert back to its permanent shape once heated again above its transition temperature. This process is often referred to as a thermal “shape recovery cycle” and is used in both the actuation of SMP (Shape Memory Polymer) structures, and to characterize their behavior [11, 16, 17].

Although shape memory polymers can be prepared using various methods, recent efforts have been concentrated on their production via additive manufacturing. The conjunction of shape memory polymers and additive manufacturing has resulted in what is commonly known as 4D printing. Multiple works have shown the use of commercially available shape memory polymers intended for use in injection molding applications as feedstock for thermoplastic additive manufacturing techniques [18-20]. In the case of vat polymerization, shape memory polymers have been formulated using different monomer units. Shape memory polymer formulations for vat polymerization techniques include precursors such as: polycaprolactone [21], epoxy acrylates [22], tert-butyl acrylate [23], and more [24, 25]. In fact, Inverardi et al observed the shape memory effect in a commercially available photopolymer resin [26]. Here, they found the photopolymer resin Clear GPCL-04 (Formlabs, Somerville, MA, USA) exhibited a shape recovery ratio of 98-99%, on a broad transition temperature range (from 40 to 100°C) on the printed material.

Additional work on this field has displayed structures with morphing capabilities representing a smart platform for future actuating mechanical/biomedical devices, as well as elements to filter vibrations and acoustic noises [27, 28]. A study performed by Zolfafharian et al [29] showed that the incorporation of a topological optimization on printed soft actuators can provide structures with a favorable internal architecture and an efficient performance. An extensive modeling work has also been carried out on the morphing capabilities of printed shape memory polymers to engineer novel design with customized functionalities and applications [27, 28]. Similarly, a preceding modeling work based on FEA, numerical, and analytical has been performed on shape memory polymers assisted by a vascular thermal mechanism to provide morphing structures [30-32]. These efforts have provided an optimization platform in terms of fixity and recovery.

For the fabrication of electrically functional components, polymer metalization seems to be a promising approach to produce conductive polymers. Various scientific works have concentrated on the integration of printed polymers and conductive metals. The addition of carbon nanotubes (CNT) to polymer blends has been widely examined for the printing process of conductive polymers [33-36]. However, this approach ultimately results in relatively poor conductance of the resulting polymer blend. The performance of these composites can vary, ranging in electrical conductivity from 1.6×10^{-2} to 81 S/m [37].

Another approach to create conductive polymer parts fabricated via 3D printing is the deposition of conductive metals onto the surface. Electroless deposition of copper ions has been investigated by multiple researchers [38-41]. This approach results in a thin layer of metal ions deposited on the surface of the parts. Lee et al [41] showed that the incorporation of an electrodeposited metal layer on the surface of the polymer can result in a conductivity of 3.8×10^5 S/cm. A similar approach

consists of using standard electroplating baths to deposit copper on the surface. Here, the surface of the polymer parts must first be made of a semi-conductive phase that can be achieved by using some form of conductive ink or coating. This technique was carried out by Angel et al. by using a semi conductive filament, followed by electroplating copper onto the surface [42].

The present work aims to harness the advantages of additive manufacturing and shape memory materials for the design of functional electromagnetic components. To achieve this, a variety of VPP polymer resins blends were investigated to determine the optimal blend for printing a shape memory polymer. An additional metallization of this shape memory polymer was carried out to determine if the printed shape memory polymers could behave as conductors. Finally, several antennas were manufactured and examined for the feasibility of this approach to fabricate functional antennas using additive manufacturing. The combination of these previous approaches represents a novel manufacturing process where a SMP is manufactured by a VPP technology followed by a controlled metallic coating to yield a smart lightweight antenna. At the present no morphing antennas have been studied throughout the specific procedure addressed in this work. The purpose of this research program is to create smart antennas for addressing multi-band operation, impedance matching, and pattern synthesis via real-time reconfiguration. This could lead to cost and space savings in applications where multiple antennas are normally needed to cover each band.

2. Materials and Methods

2.1 Materials and Methods

For this work, a commercially available methacrylate photopolymer resin, Clear RS-F2-GPCL-04 (Formlabs, Somerville, MA, USA) was utilized as the basis for investigation. While this material exhibits the thermal shape memory effect, it possesses a rather brittle behavior both at room temperature and elevated temperature [26]. To mitigate the brittleness of this material, an elastomeric acrylate photopolymer resin, Elastic RS-F2-ELCL-01, (Formlabs) was blended with the Clear resin to improve upon the brittle behavior. Overall, five resin mixtures were examined, with the mass fraction of Elastic material in each mixture ranging from 0 (100% Clear resin) to 0.4 (60% Clear, 40% Elastic). Each mixture was mixed with a laboratory stand mixer for 5 minutes, and then placed in an ultrasonic bath for 60 minutes at 40°C.

Following the mixing, all resin mixtures were printed on a Form 2 SLA 3D printer (Formlabs, Somerville, MA, USA). Print files were prepared using the provided PreForm software, and all prints were conducted using the printer's "open-mode" at a layer height of 100 μm . After printing, the samples were washed in isopropyl alcohol (IPA) for ten minutes, and allowed to fully dry. Then parts were placed in an ultraviolet curing chamber (Formlabs) and post cured for 20 minutes at 60°C following the protocol established by the supplier [43].

2.2 Thermal and Mechanical Testing

To investigate the mechanical performance of the manufactured samples, both uniaxial tensile and flexural tests were used. Both tests were conducted on a minimum of four samples to determine a statistical average and standard deviation. Both tests were also conducted at room temperature, on a universal testing instrument (Instron 5967) equipped with a load cell and moving

cross-head. Strain for both tests was taken as cross head displacement. Flexural tests were conducted in the three-point bend setup according to ASTM D790 (West Conshohocken, PA, USA). Flexural test specimens (3 mm × 10 mm × 100 mm) were tested at a compression rate of 5 mm/min. Uniaxial tensile tests were tested using the type IV dogbone, based on ASTM D638, at an extension rate of 2 mm/min.

In order to examine the change in mechanical response with respect to temperature, a dynamic mechanical analysis (DMA) was employed. Thin rectangular samples (~ 30 mm × 5 mm × 0.5 mm), were tested using a Seiko DMS 200 (SII, Tokyo, Japan). Samples were tested from 25 - 200°C at a frequency at 1 Hz, and displacement of 10 μm. The entire cycle was repeated, and the second dynamic cycle was utilized in measuring the storage modulus, loss modulus, and tangent delta of the material.

In addition to the DMA, a differential scanning calorimetry (DSC) was used to investigate other thermal events within the material. Here, small samples (5-10 mg) were sealed in aluminum sample pans with lids. Samples were placed in a Perkin-Elmer Hyper DSC (Waltham, MA, USA), and scanned from 0 to 200°C at a rate of 10 °C/min. The sample was held under an isothermal for 5 min, and cooled to 0°C at the same rate. Once again, samples were scanned twice, and the second heating ramp was used in calculating the glass transition temperature (T_g) over the exhibited broad glass transition.

2.3 Shape Memory Properties

For shape memory polymers, the two most defining characteristics are the shape recovery and shape fixity ratio. Firstly, the shape recovery defines how effective the polymer part is at recovering the permanent shape after an applied deformation. Secondly, the measure of how capable the polymer is at storing a specific deformation is the shape fixity ratio. From an applied stress, and therefore strain of deformation, the shape fixity ratio can be described by equation (1) and the shape recovery as described by equation (2):

$$R_f = \frac{\epsilon_p(N)}{\epsilon_m} \quad (1)$$

$$R_r = \frac{\epsilon_m - \epsilon_p(N)}{\epsilon_m - \epsilon_p(N - 1)} \quad (2)$$

where, ϵ_m is the maximum strain applied, ϵ_p is the stress-free recovered strain, and N represents the cycle number [10].

2.4 Electroplating Process and Antenna Fabrication

The electroplating process of the printed SMP parts was carried by soaking the specimens in a bath of isopropyl alcohol (240 g) and graphite (1.5 g). After soaking for 24 hours, the parts were removed and allowed to dry. The desired sections of the 3D printed parts that are intended to be electroplated are coated with a graphene based conductive ink, purchased from Working Ink, UK [44]. Finally, the conductive ink-coated SMPs were placed in an electroplating solution to deposit copper ions on the coated areas. The electroplating solution consisted of 40 g of copper sulfate, 7 g of H₂SO₄ (97% by mass), and 200 ml of deionized water. The SMP parts were placed in the

electroplating bath and connected to a DC power supply at 0.2 Volts for ~2 hour, or until a continuous layer of copper was deposited on the surface. Figure 1 shows an electroplated spiral on a 3D printed part. This process allows for the deposition of copper on selected areas. An helical antenna was subsequently printed and its radiofrequency performance evaluated as a function of their morphing behavior. Figure 2 displays the printed helical structure that was plated with copper as the conductive phase.



Figure 1 3D printed parts used on the work for investigating the copper electroplating process. The as-printed shape memory polymer (left), the conductive coating applied only to a spiral pattern on the part (middle), and the copper traces after electroplating the ink (right).



Figure 2 Manufactured 3D printed SMP helical antenna to be electroplated with copper for using it as a smart antenna.

The conductivity of the electroplated copper was here measured by coating a square section and subjecting it to a four-point probe test to measure the sheet resistance. The plated parts were placed on the platform of a Niko Eclipse ME600 inspection microscope. An applied DC current was driven using a Keithley 2410 SMU between the outer two probes and a voltmeter measured the voltage difference between the inner two probes. A current of 10-100 mA was applied here [45]. The sheet resistance was then determined using equation (3).

$$\rho_s = \frac{V}{I} 4.534 [\Omega \cdot \text{sq}] \quad (3)$$

The fabricated antennas were analyzed using a virtual network analyzer (VNA) to elucidate their S_{11} parameters under 1-port analysis. An Agilent Technologies (Santa Clara, CA) E5061B virtual network analyzer was used to examine the antenna in the frequency range of 100 KHz to 3 GHz. All of the printed antennas were embedded with a 50-ohms coaxial SMA connector to connect the antenna to the VNA. For comparison, the metal structures of each fabricated antenna were simulated using Ansys (Canonsburg, PA) HFSS. The modeling used polyethylene as the dielectric substrate, with a relative permittivity of 2.25, a dielectric loss tangent 0.001, and a mass density of 930 kg/m³.

3. Results and Discussion

The mechanical and rheological properties of the manufactured polymers were evaluated to characterize their performance under the temporary and permanent shape configurations. A metallic phase was incorporated into the printed parts and their radiofrequency measured and simulated following a thermal activation to induce a conformational shape change on the structures.

3.1 Mechanical Properties

The mechanical response of the polymer blends was first examined under uniaxial tensile tests. It was observed that the incorporation of the elastic resin resulted in a decrease in the ultimate tensile strength and Young's modulus for all polymer blends containing more than 20% by mass of the Elastic resin. As seen in Figure 3, the polymer blend consisting of only 10% by mass elastic resin exhibited measured values of tensile strength, Young's modulus, and strain at failure similar to that of the unmodified Clear resin. Indicating that this polymer blend was governed solely by the clear resin in the matrix. However, once the mass fraction of the Elastic resin reached a value of 0.2 and higher, these properties consistently dropped. It was also observed that the incorporation of Elastic resin in the polymer blend did improve the strain at failure. As seen in Figure 3, the strain at failure for the polymer blend consisting of 0.4 mass fraction of Elastic resin exhibited a strain at break of 0.15 mm/mm, a value five times higher than the unmodified polymer of 0.03 mm/mm. Overall, this test indicated the brittle behavior of the Clear resin could be mitigated with an elastic resin at concentrations above 0.2 mass fraction.

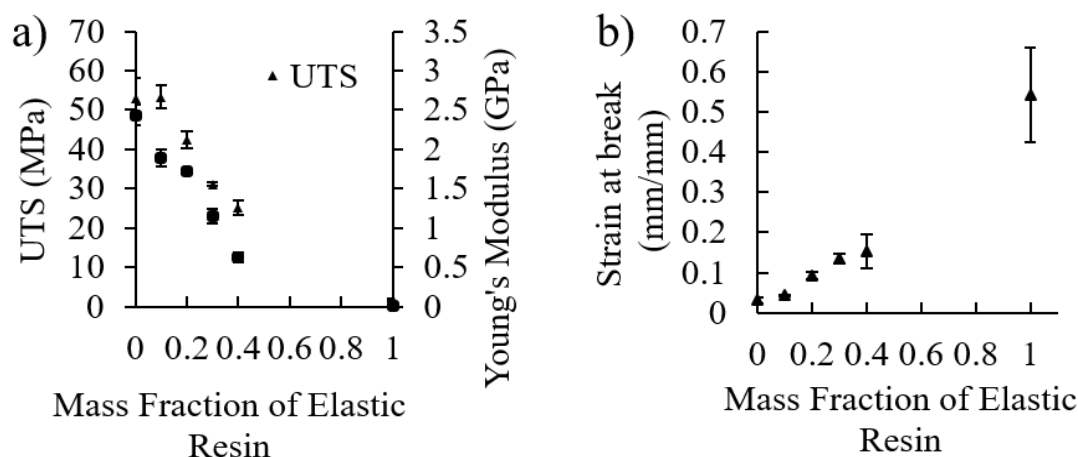


Figure 3 Mechanical properties of the printed polymers. (a) The ultimate tensile stress and Young’s modulus of the examined polymer blends under uniaxial conditions. (b) The strain at break measured for each of the examined blends.

The polymer blends were also examined under flexural conditions in a 3-point bend configuration and similar observations from the tensile test were observed here. The sample containing only 0.1 mass fraction of the Elastic Resin exhibited a similar flexural strength to the unmodified clear resin. However, once the mass fraction of the Elastic resin increased above 0.2, the flexural strength decreased (see Figure 4). The sample containing the highest amount of Elastic resin resulted in a flexural strength of 23.3 MPa (± 0.67 MPa), which was considerable lower than the flexural strength measured in the neat Clear material of 62.2 MPa (± 3.2 MPa).

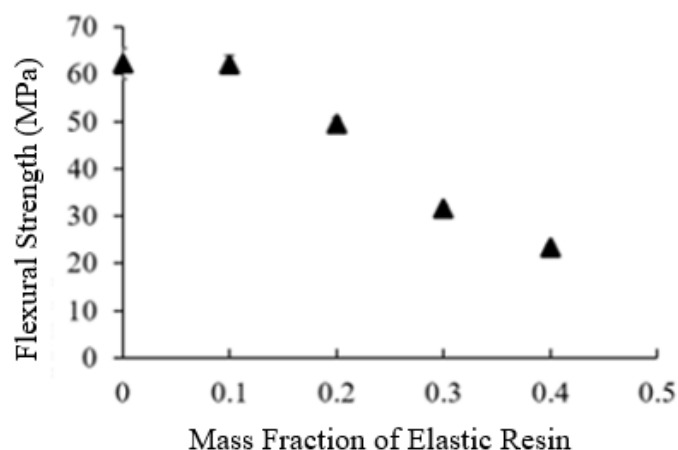


Figure 4 Flexural strength of each of the modified polymer blends investigated in this work.

3.2 Thermal Properties

The transition temperature of these polymer blends is an important property if these polymers are to be exploited as smart actuators or morphing antennas. These polymer blends were first examined under differential scanning calorimetry. Here, it was found that the T_g of the polymer blends ranged from 60 to 80°C, with no clear trends distinguishing these polymer blends (as seen in

Table 1). Other studies have provided T_g values of the same Clear (unmodified) resin in the 53°C to 107.2°C range [26, 46]. The amorphous nature of this material results in a broad glass transition region, which yields an unreliable glass transition temperature.

Table 1 The glass transition temperatures of the investigated printed polymers determined by DSC and DMA.

<i>Sample</i>	<i>T_g by DSC (°C)</i>	<i>T_g by DMA (°C)</i>
<i>0E</i>	60.43	97.50
<i>10E</i>	84.97	96.92
<i>20E</i>	67.35	93.45
<i>30E</i>	76.33	87.62
<i>40E</i>	80.03	80.09

To better investigate the mechanical response of the formulated polymer blends with respect to temperature, dynamical mechanical analysis was used to determine the glass transition temperature. From the peak of the tangent delta curve, the glass transition temperatures were determined (see Table 1). It was noted that the polymer blends containing 0 to 0.2 mass fraction of the Elastic resin by mass exhibited a glass transition temperature within five degrees of the neat Clear resin (97.5°C). This suggests a degree of miscibility between the two systems on the 0-0.2 Elastomer mass fraction range. However, polymer blends containing 0.3 and 0.4 of the Elastic resin by mass exhibited a larger difference in the glass transition temperature (> 10°C). Overall, the polymer blends showed a transition temperature between 80 and 100°C, this glass transition was useful in determining the temperature used on the shape recovery and temporary deformation of the morphing structures.

3.3 Morphing Properties

The shape recovery properties were investigated for each of the polymer blends. In this case, each sample underwent twenty shape recovery cycles in a thermomechanical analyzer. This data was used to determine the shape fixity and shape recovery ratio by equations (1) and (2) respectively. Here, it was found that all of the polymer blends exhibited high values of shape recovery (above 0.95) after the first cycle (see Figure 5). The lower values of shape recovery examined in the first cycle are attributed to an incomplete cross linkage of the polymer network, although the curing procedure was based on the supplier's recommendation. As was the case of other thermal analysis techniques, the additional heat of the first cycle allows for complete polymerization and crosslinking of the samples.

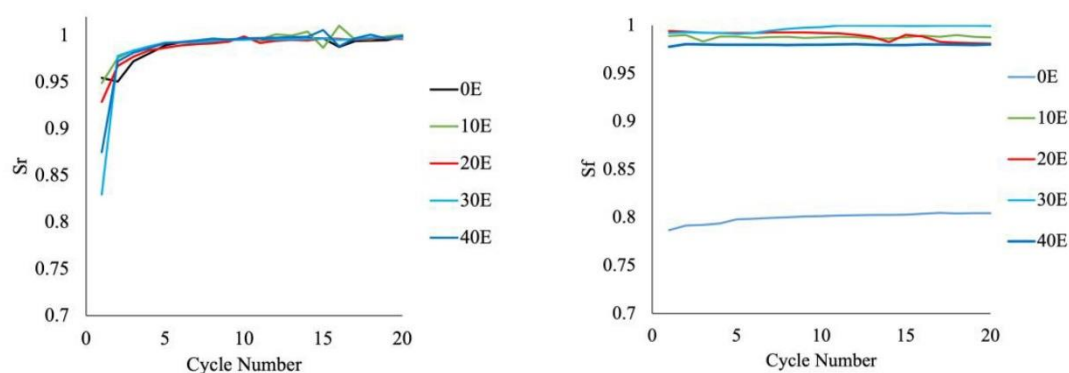


Figure 5 Shape memory properties of the printed polymer mixtures. (a) The shape recovery ratios. (b) The shape fixity ratio.

The figure also shows that all the examined polymer blends containing the Elastic resin exhibited an excellent shape recovery and shape fixity properties. However, it was observed that the unmodified polymer blend of Clear (0E) resin exhibited an inferior shape fixity ratio (0.78-0.8) when compared to the remaining polymer blends. It is widely known that the hard and soft segments in SMPs above and below the switching temperature contribute to the shape fixity phenomena. Indeed, it is well known that the soft segment phase is related to the shape fixity of SMPs, while the hard segment phase greatly affects the shape recovery [47]. The temporary shape is commonly fixed by the hardening of the soft segments, since this phase provides the restriction against relaxation of the stretched/deformed system [47]. Thus, the lack of soft segments provided by the elastomer resin, resulted in an inferior fixity performance.

Overall, the thermal, rheological and mechanical results suggest that the modified polymer blends exhibited consistent shape recovery and shape fixity and are attractive candidates for actuating applications.

From these analyses, it was clear that the addition of elastic resin mitigated the brittleness of the polymer blends while retaining the shape memory properties inherent to the Clear resin. However, the printability of each polymer blend was inconsistent due to the lack of adjustability of the printing parameters on the Form 2 printer. Polymer blends containing a mass fraction of 0.3 and 0.4 Elastic resin showed a higher occurrence of print defects, and print failures in the manufacturing process. As such, the blend of 0.2 mass fraction Elastic resin was chosen as the superior candidate for further investigation on the antenna designs. This polymer blend exhibited a high shape recovery (0.99 after twenty cycles), a distinct glassy behavior at room temperature (Young's Modulus of 1.71 GPa), a strain at failure three times higher than the unmodified polymer, and acceptable printability and processing features.

3.4 Functional Metallized 3D Printed Structures

The printed resin based on the 0.2 Mass fraction of Elastic resin was subjected to an electroplating process. The quality of the attached copper onto the printed substrates was observed under an optical and SEM microscopy. Figure 6 shows the coated and uncoated printed parts, where it can be observed the smooth covering of copper and the coalescence of metallic particles to yield

a conductive system. It was found that the coated parts exhibited a sheet resistance of $0.2845 \Omega/\text{sq}$ determined via four-point probe analysis.

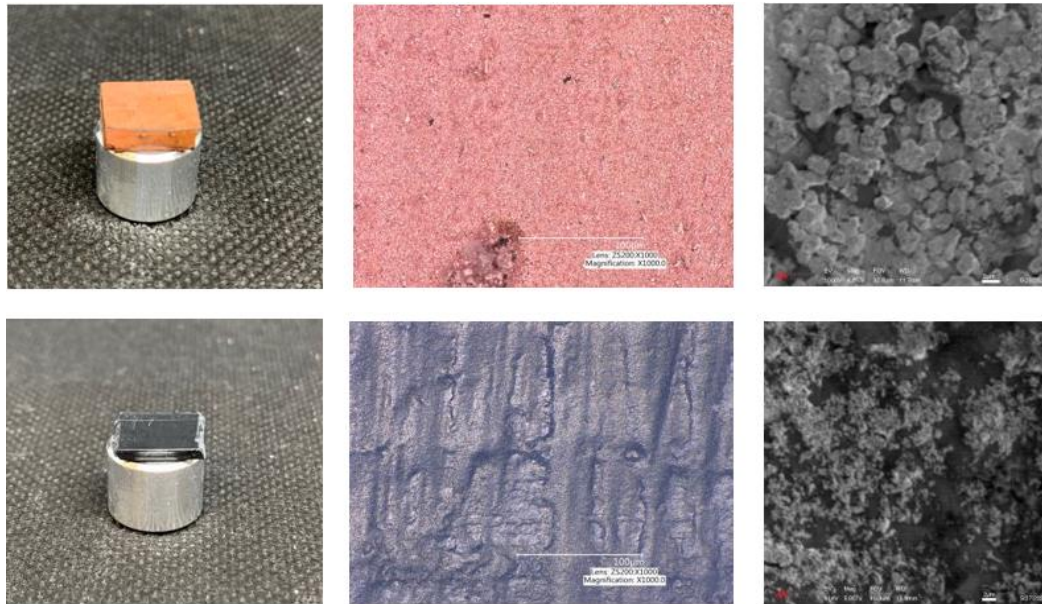


Figure 6 Optical and SEM observation of the printed resins following an electroplating copper process. Included in the figure is the plain resin as reference.

The SEM was utilized to investigate the copper coating, and determine the sheet thickness of the plated region, and upon examination of the cross-sectional sample, it was found that the thickness of the copper plating was $\sim 1 \mu\text{m}$. This resulted in a bulk resistivity of $2.845 \times 10^{-7} \Omega \cdot \text{m}$ for the copper plating, compared to the bulk resistivity for pure copper, which is $1.7 \times 10^{-8} \Omega \cdot \text{m}$; a value commensurable to other recent works [48, 49].

To examine the functionality of the printed antenna, the helical antenna was examined using a virtual network analyzer. The antenna was adhered to a coaxial connector and fabricated using a flat sheet of copper as the ground plane. Here, the part was heated above its T_g (using boiling water - 100°C), and once the SMP entered into its rubbery state, the antenna was deformed to yield an extended spiral. At this point, the part was cooled while keeping it stretched. Once at room temperature, its radiofrequency was tested. A subsequent heating step was used, which resulted in the antenna recovering its compressed permanent state. After allowing it to reach room temperature, its radiofrequency was again evaluated. In practical cases, the activation of the SMP system could be carried out by incorporating D-shape optical fibers capable of providing near infrared light to activate the SMP as shown by Herath et al [50]. An alternative activation process on more realistic sceneries could be integration of diminutive thermo vascular arrays to induce activation. In either case, the incorporation of a thermal or a photo-thermal source element needs to be incorporated in the electromagnetic modeling of the antenna to ensure the design of the system is adjusted accordingly to provide the desired performance.

The helical antenna was simulated and compared to the measured S_{11} parameters. The antenna is modeled as a bulk copper surface, 30 micrometers thick surrounding a dielectric core. Though the thickness of the conductive coating in the simulation is several skin depths for bulk copper at 1.5 GHz, significant inaccuracy in resonant frequency was not observed in the temporary part geometry

of Figure 7a. The figure also shows the antenna under the permanent conformal stage (Figure 7b). A narrowing of the resonance peak was observed at 1.6 GHz and a more uniform rejection was observed below 1.5 GHz. Inaccuracy in the return loss of the fixed antenna of Figure 7b can be attributed to slight variations in the geometry of the simulation relative to the final part. This can cause a mismatch in the attenuation of the current distribution at the feed point between the simulated and tested cases. Included in Figure 7 is the shape recovery ratio of the manufactured antenna after being subjected to several adaptive cycles following the aforementioned thermo-mechanical process. The figure shows that less than 1% of the shape memory effect has been lost after 60 cycles. Here, two specific locations were selected on the antenna, and using a digital caliper, the shape recovery was evaluated. It seems that some small deviations were encountered during the measuring process, which resulted in some reading discrepancies. However, the overall trend of the system appears to show a relatively constant structural recovery on the number of cycles here investigated.

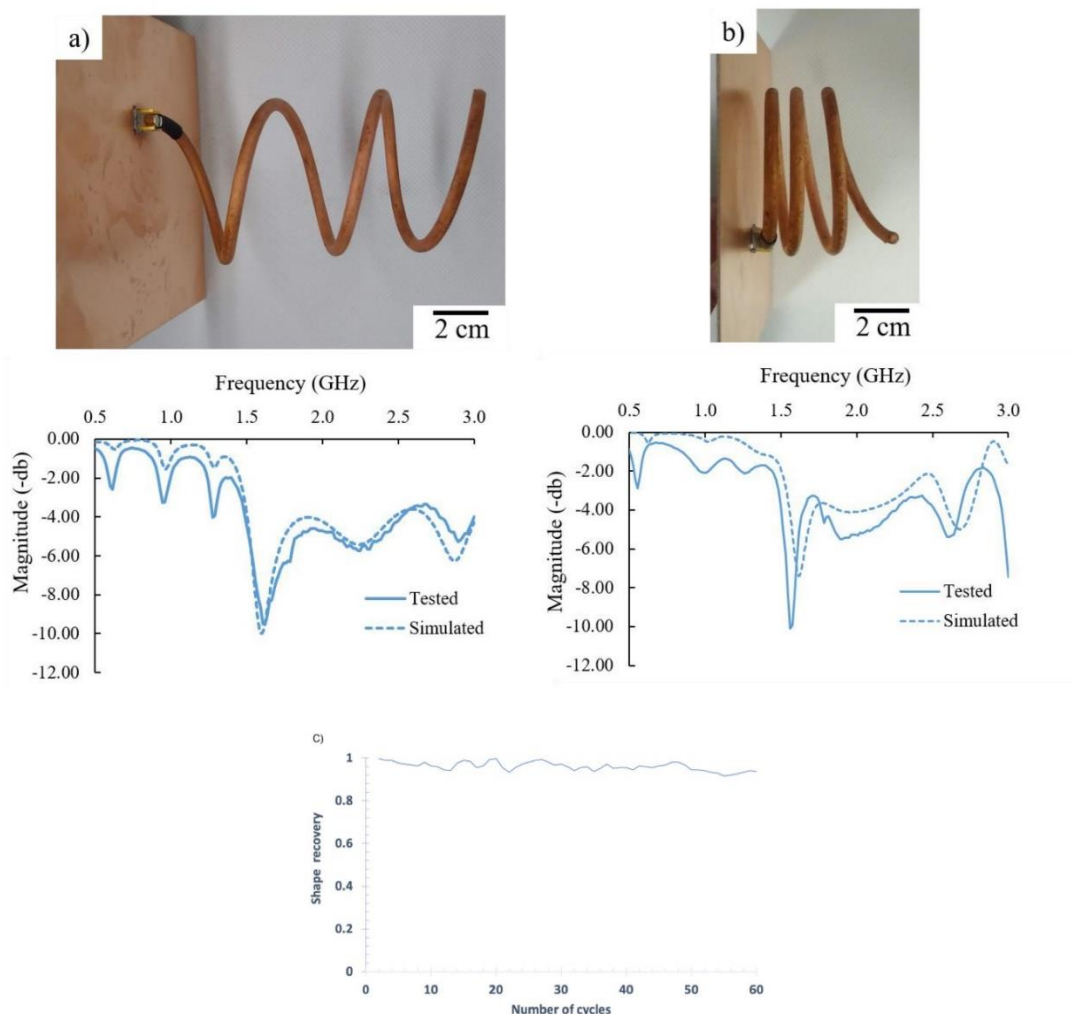


Figure 7 3D printed shape memory polymer coated in copper, (a) the helix with a total axial length of 100 mm, (b) a total axial length of 40 mm. The S_{11} parameter plots obtained from the use of the VNA are shown below each helical antenna. Included in the figure is the shape recovery of the antenna after being subjected to several morphing cycles.

It is worth noticing that although relatively long endurance studies have been performed on SMPs [51], an extensive and comprehensive cycle-analysis on the smart 4D printed electroplated parts needs to be further investigated to expand the understand the polymer degradation mechanisms due to thermal and UV-Vis effects as well as potential interfacial and endurance features on the metal phase due to fatigue conditions. These detrimental mechanisms can deteriorate the structural configuration of the system and the conductivity of the antenna, which would result in a low electromagnetic performance.

4. Conclusion

This research paper investigated the use of a photopolymerization technique to manufacture shape memory polymer systems as the structures of morphing antennas based on a mixture of Clear and Elastic resins. The printed parts were mechanically, thermally and rheologically characterized to evaluate the effect of their different blending resin ratios. All polymer blends consisting of more than 20% by mass of Elastic resin exhibited a consistent decrease in tensile and flexural strength, but showed an increase in the strain at break. Out of the four polymer blend resins investigated, the 0.2 mass fraction of Elastic was chosen for the antenna design based on its mechanical performance. This blend showed good printability and processability features, as well as a high shape recovery ratio (0.99 after twenty cycles), and a strain at failure three times higher than the unmodified polymer. The printed morphing parts were designed as a helical configuration. These antennas were copper plated, resulting in structures with a bulk resistivity on the copper of $2.845 \times 10^{-7} \Omega \cdot m$. The electroplated process was examined via four-point probe analysis, resulting in a sheet resistance of $0.2845 \Omega / sq$. The radiofrequency of the helical antenna was evaluated in a VNA unit and simulated using the HFSS Ansys software. The modeling appeared to follow the actual electromagnetic profile recorded by the VNA testing, suggesting that pre-selected design can be simulated in the future for targeting specific radiofrequency responses. The ability to modulate return loss via antenna deformation can be manifested for many different geometries. This new flexibility in antenna design may find application for passive remote sensing or in communications applications. This work has shown that the change in configuration in the lightweight polymeric based morphing antennas results in a unique electromagnetic response, a feature of interest to the communications field where multi-frequencies signals are required.

Author Contributions

Trenton Cersolli: Performing tests, evaluation of results, manuscript writing. Muneer Barnawi: Performing tests, data collection, evaluation of results. Kerry Johnson: Modeling of antenna and data analysis. Edward Burden: Modeling of antenna and supervision of the antenna's modeling. Dr. Frank Li: Manuscript writing, evaluation of results, and supervision of antenna testing. Dr. Eric MacDonald: Manuscript writing and 3D printing supervision. Dr. Pedro Cortes: Writing the manuscript, conceptualization, and direction of the project.

Funding

The authors would like to acknowledge the Ohio Federal Research Network and the Air Force ADMETE program for funding this work.

Competing Interests

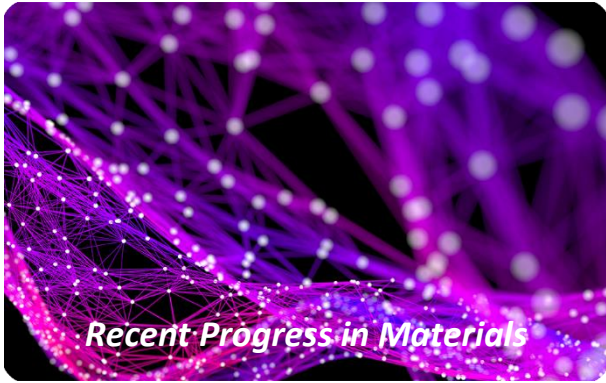
The authors have declared that no competing interests exist.

References

1. Durakovic B. Design for additive manufacturing: Benefits, trends and challenges. *Period Eng Nat Sci.* 2018; 6: 179-191.
2. Bandyopadhyay A, Heer B. Additive manufacturing of multi-material structures. *Mater Sci Eng R Rep.* 2018; 129: 1-16.
3. Thomas DS, Gilbert SW. Costs and cost effectiveness of additive manufacturing. *NIST Spec Pub.* 2014; 1176: 12.
4. Deckers J, Vleugels J, Kruth JP. Additive manufacturing of ceramics: A review. *J Ceram Sci Technol.* 2014; 5: 245-260.
5. Herzog D, Seyda V, Wycisk E, Emmelmann C. Additive manufacturing of metals. *Acta Mater.* 2016; 117: 371-392.
6. Bourell D, Kruth JP, Leu M, Levy G, Rosen D, Beese AM, et al. Materials for additive manufacturing. *CIRP Ann.* 2017; 66: 659-681.
7. Revilla León M, Özcan M. Additive manufacturing technologies used for processing polymers: Current status and potential application in prosthetic dentistry. *J Prosthodont.* 2019; 28: 146-158.
8. Cao W, Cudney HH, Waser R. Smart materials and structures. *Proc Natl Acad Sci USA.* 1999; 96: 8330-8331.
9. Theato P, Sumerlin BS, O'Reilly RK, Epps III TH. Stimuli responsive materials. *Chem Soc Rev.* 2013; 42: 7055-7056.
10. Melly SK, Liu L, Liu Y, Leng J. Active composites based on shape memory polymers: Overview, fabrication methods, applications, and future prospects. *J Mater Sci.* 2020; 55: 10975-11051.
11. Leng J, Lan X, Liu Y, Du S. Shape-memory polymers and their composites: Stimulus methods and applications. *Prog Mater Sci.* 2011; 56: 1077-1135.
12. Jape S, Garza M, Ruff J, Espinal F, Sessions D, Huff G, et al. Self-foldable origami reflector antenna enabled by shape memory polymer actuation. *Smart Mater Struct.* 2020; 29: 115011.
13. Zhang R, Guo X, Liu Y, Leng J. Theoretical analysis and experiments of a space deployable truss structure. *Compos Struct.* 2014; 112: 226-230.
14. Liu Y, Du H, Liu L, Leng J. Shape memory polymers and their composites in aerospace applications: A review. *Smart Mater Struct.* 2014; 23: 023001.
15. Ze Q, Kuang X, Wu S, Wong J, Montgomery SM, Zhang R, et al. Magnetic shape memory polymers with integrated multifunctional shape manipulation. *Adv Mater.* 2020; 32: e1906657.
16. Tobushi H, Okumura K, Hayashi S, Ito N. Thermomechanical constitutive model of shape memory polymer. *Mech Mater.* 2001; 33: 545-554.
17. Lan X, Liu Y, Lv H, Wang X, Leng J, Du S. Fiber reinforced shape-memory polymer composite and its application in a deployable hinge. *Smart Mater Struct.* 2009; 18: 024002.
18. Cersoli T, Cresanto A, Herberger C, MacDonald E, Cortes P. 3D printed shape memory polymers produced via direct pellet extrusion. *Micromachines.* 2021; 12: 87.

19. Villacres J, Nobes D, Ayranci C. Additive manufacturing of shape memory polymers: Effects of print orientation and infill percentage on mechanical properties. *Rapid Prototyp J.* 2018; 24: 744-751.
20. Raasch J, Ivey M, Aldrich D, Nobes DS, Ayranci C. Characterization of polyurethane shape memory polymer processed by material extrusion additive manufacturing. *Addit Manuf.* 2015; 8: 132-141.
21. Invernizzi M, Turri S, Levi M, Suriano R. 4D printed thermally activated self-healing and shape memory polycaprolactone-based polymers. *Eur Polym J.* 2018; 101: 169-176.
22. Shan W, Chen Y, Hu M, Qin S, Liu P. 4D printing of shape memory polymer via liquid crystal display (LCD) stereolithographic 3D printing. *Mater Res Express.* 2020; 7: 105305.
23. Choong YYC, Maleksaeedi S, Eng H, Yu S, Wei J, Su PC. High speed 4D printing of shape memory polymers with nanosilica. *Appl Mater Today.* 2020; 18: 100515.
24. Zarek M, Layani M, Cooperstein I, Sachyani E, Cohn D, Magdassi S. 3D printing of shape memory polymers for flexible electronic devices. *Adv Mater.* 2016; 28: 4449-4454.
25. Ge Q, Sakhaei AH, Lee H, Dunn CK, Fang NX, Dunn ML. Multimaterial 4D printing with tailorable shape memory polymers. *Sci Rep.* 2016; 6: 31110.
26. Inverardi N, Pandini S, Bignotti F, Scalet G, Marconi S, Auricchio F. Sequential motion of 4D printed photopolymers with broad glass transition. *Macromol Mater Eng.* 2020; 305: 1900370.
27. Bodaghi M, Noroozi R, Zolfagharian A, Fotouhi M, Norouzi S. 4D printing selfmorphing structures. *Materials.* 2019; 12: 1353.
28. Noroozi R, Bodaghi M, Jafari H, Zolfagharian A, Fotouhi M. Shape-adaptive metastructures with variable bandgap regions by 4D printing. *Polymers.* 2020; 12: 519.
29. Zolfagharian A, Denk M, Bodaghi M, Kouzani AZ, Kaynak A. Topology-optimized 4d printing of a soft actuator. *Acta Mech Solida Sin.* 2020; 33: 418-430.
30. Terzak J, Cortes P, McClung AJW, Baur JW. Modeling of the bending actuation of shape memory composites. *Mater Sci.* 2012: 575-582.
31. Cortes P, McClung AJW, Sakulich J, Baur JW. The relationship between constituent property and bending actuation of shape memory composites. In: *Behav Mech Multifunct Mater Compos 2012.* SPIE. 2012; 8342: 230-241. doi: 10.1117/12.914153.
32. Cortes P, Terzak J, Kubas G, Phillips D, Baur JW. The morphing properties of a vascular shape memory composite. *Smart Mater Struct.* 2013; 23: 015018.
33. Daver F, Baez E, Shanks RA, Brandt M. Conductive polyolefin–rubber nanocomposites with carbon nanotubes. *Compos Part A Appl Sci Manuf.* 2016; 80: 13-20.
34. Chizari K, Arjmand M, Liu Z, Sundararaj U, Therriault D. Three-dimensional printing of highly conductive polymer nanocomposites for EMI shielding applications. *Mater Today Commun.* 2017; 11: 112-118.
35. Gnanasekaran K, Heijmans T, van Bennekom S, Woldhuis H, Wijnia S, de With G, et al. 3D printing of CNT- and graphene-based conductive polymer nanocomposites by fused deposition modeling. *Appl Mater Today.* 2017; 9: 21-28.
36. Postiglione G, Natale G, Griffini G, Levi M, Turri S. Conductive 3D microstructures by direct 3D printing of polymer/carbon nanotube nanocomposites via liquid deposition modeling. *Compos Part A Appl Sci Manuf.* 2015; 76: 110-114.
37. Su X, Li X, Ong CYA, Heng TS, Wang Y, Peng E, et al. Metallization of 3D printed polymers and their application as a fully functional water-splitting system. *Adv Sci Lett.* 2019; 6: 1801670.

38. Bernasconi R, Credi C, Tironi M, Levi M, Magagnin L. Electroless metallization of stereolithographic photocurable resins for 3D printing of functional microdevices. *J Electrochem Soc.* 2017; 164: B3059.
39. Zhan J, Tamura T, Li X, Ma Z, Sone M, Yoshino M, et al. Metal-plastic hybrid 3D printing using catalyst-loaded filament and electroless plating. *Addit Manuf.* 2020; 36: 101556.
40. Fan Q, Gao Y, Zhao Y, Yang Q, Guo L, Jiang L. Fabrication of diamond-structured composite materials with Ni-P-diamond particles by electroless plating. *Mater Lett.* 2018; 215: 242-245.
41. Lee S, Wajahat M, Kim JH, Pyo J, Chang WS, Cho SH, et al. Electroless deposition-assisted 3D printing of micro circuitries for structural electronics. *ACS Appl Mater Interfaces.* 2019; 11: 7123-7130.
42. Angel K, Tsang HH, Bedair SS, Smith GL, Lazarus N. Selective electroplating of 3D printed parts. *Addit Manuf.* 2018; 20: 164-172.
43. Form Cure time and temperature settings [Internet] [cited date 2022 April 21]. Available from: https://support.formlabs.com/s/article/Form-Cure-Time-and-Temperature-Settings?language=en_US.
44. Shop [Internet] [cited date 2021 March 28]. Available from: <https://secure.workingink.co.uk/working-ink-shop/>.
45. Waremra RS, Betaubun P. Analysis of electrical properties using the four point probe method. *E3S Web Conf.* 2018; 73: 13019.
46. Mendes Felipe C, Patrocinio D, Laza JM, Ruiz Rubio L, Vilas Vilela JL. Evaluation of postcuring process on the thermal and mechanical properties of the Clear02TM resin used in stereolithography. *Polym Test.* 2018; 72: 115-121.
47. Abdullah SA, Jumahat A, Abdullah NR, Frommann L. Determination of shape fixity and shape recovery rate of carbon nanotube-filled shape memory polymer nanocomposites. *Procedia Eng.* 2012; 41: 1641-1646.
48. Schuster CE, Vangel MG, Schafft HA. Improved estimation of the resistivity of pure copper and electrical determination of thin copper film dimensions. *Microelectron Reliab.* 2001; 41: 239-252.
49. Yung WKC, Sun B, Huang J, Jin Y, Meng Z, Choy HS, et al. Photochemical copper coating on 3D printed thermoplastics. *Sci Rep.* 2016; 6: 31188.
50. Herath M, Epaarachchi J, Islam M, Zhang F, Leng J, Fang L, et al. Remote actuation of light activated shape memory polymers via D-shaped optical fibres. *Smart Mater Struct.* 2020; 29: 047001.
51. Kong D, Xiao X. High cycle-life shape memory polymer at high temperature. *Sci Rep.* 2016; 6: 33610.



Enjoy *Recent Progress in Materials* by:

1. [Submitting a manuscript](#)
2. [Joining in volunteer reviewer bank](#)
3. [Joining Editorial Board](#)
4. [Guest editing a special issue](#)

For more details, please visit:

<http://www.lidsen.com/journals/rpm>